AAS 18-410

INITIAL ORBIT DETERMINATION WITH VELOCITY VECTORS AND ANGLES

Courtney L. Hollenberg* **and John A. Christian†**

Classical methods of inital orbit determination (IOD) from Earth-bound observations are well established. Although traditional methods utilize range, position, and angle measurements, advancements in measurement techniques and sensor technologies have motivated a new class of IOD problems that utilize different parameters. Specifically, x-ray pulsar navigation (XNAV) allows for significantly more accurate measurements of an object's velocity vector than its position in the absence of an a-priori state estimate. A new method for initial orbit determination using only two velocity vectors (e.g. from XNAV) combined with their respective lines-of-sight to the central body (e.g. from sun sensors) is presented. Theoretical results are validated through numerical simulations.

INTRODUCTION

Initial orbit determination (IOD) given a limited measurement set is a classical problem of orbital mechanics. Some notable examples include angles-only IOD with bearings at three known times (methods of Laplace, Gauss, Gooding),[1–4] IOD with three position vectors (methods of Gibbs and Herrick-Gibbs),[1,2] and two position vectors and time-of-flight (Lambert's Problem).[1–3] In this work, a new orbit determination method is proposed using only two velocity estimates and their corresponding bearing measurements to the central body. This is one of a new class of velocity-based IOD problems being explored by the authors, as summarized in Fig. 1. In each of these new problems, the classic IOD problems mentioned above are reimagined where velocity information is known instead of position information (e.g. a Gibbs-equivalent problem may be posed with three velocity vectors instead of three position vectors).

An example of a system that benefits from this methodology is x-ray pulsar navigation (XNAV) which operates by observing x-ray emissions of stable millisecond pulsars.[5] The time-of-arrival (TOA) of pulses can be used to determine a relative position in the direction of the pulsar. Velocity estimates in the direction of a pulsar may be generated in a similar manner by observing the frequency of the signal and comparing it to the known period of the pulsar.

A key limitation of the technology is the requirement of an initial position estimate to resolve the pulse phase ambiguity. Since the measurement only produces a relative phase error, and there is no way of directly determining which wavefront is observed, there are multiple position solutions which are all equally feasible. However, the velocity estimate may still be generated via the frequency without requiring any a-priori knowledge of the state.

*Graduate Research Assistant, Department of Mechanical, Aerospace, and Nuclear Engineering, Rensselaer Polytechnic Institute, Troy New York 12180.

†Assistant Professor, Department of Mechanical, Aerospace, and Nuclear Engineering, Rensselaer Polytechnic Institute, Troy New York 12180.

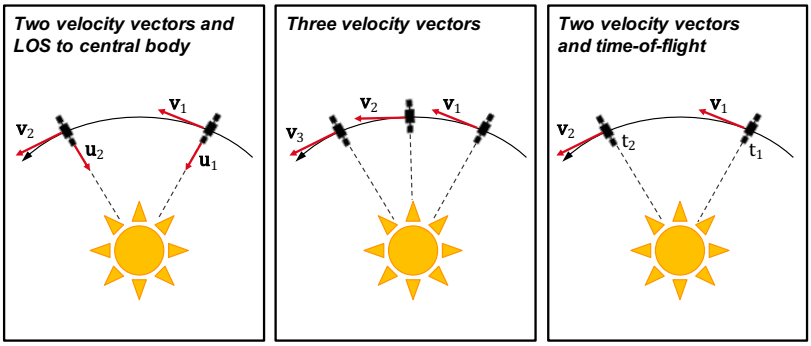

Figure 1. A new class of initial orbit determination (IOD) problems are proposed where velocity information is known. These are similar to classic IOD problems (e.g. Gibbs, Lambert), but where velocity is known instead of position.

Assuming IOD for a spacecraft in a heliocentric orbit, line-of-sight to the central body (the Sun) can be easily and inexpensively obtained with a sun sensor.

Therefore, we propose a method to solve the IOD problem by combining XNAV velocity measurements with sun sensor bearing measurements, after which the XNAV system may further refine the estimate. The end result is a robust and completely autonomous navigation system for vehicles operating in heliocentric space.

METHOD FOR INITIAL ORBIT DETERMINATION

Traditional methods of initial orbit determination exist for observations of range and angles, angles-only, position vectors and time, and mixed observations.[1,2] The following method describes a closed-form solution to the initial value problem given two velocity vectors and corresponding line-of-sight unit vectors, as shown in Fig. 2.

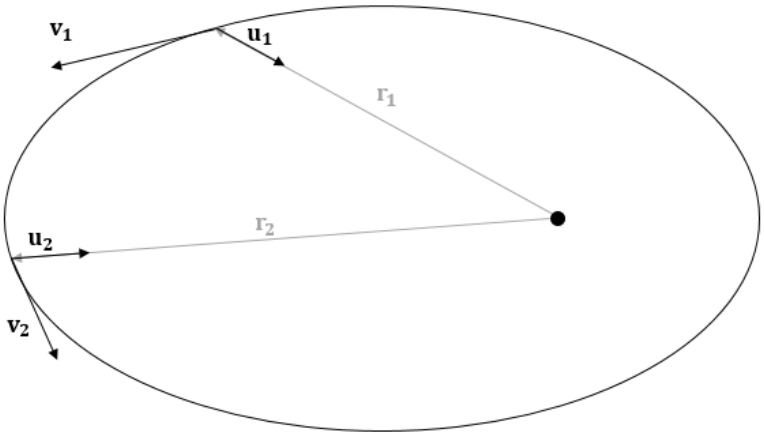

Figure 2. Geometry of IOD with velocity and line-of-sight vectors.

Given the line-of-sight to central body, $\mathbf{u}_i$, and velocity vector, $\mathbf{v}_i$, at two times, t_1 and t_2, the orbit can be fully defined by solving for the position vector at either of the two times.

The line-of-sight unit vector from the spacecraft to the central body is related to the position vectors

$$\mathbf{r}_1 = -\rho_1 \mathbf{u}_1 \qquad \mathbf{r}_2 = -\rho_2 \mathbf{u}_2 \tag{1}$$

such that the only unknowns in the problem are the ranges, $\rho_1 = \|\mathbf{r}_1\|$ and $\rho_2 = \|\mathbf{r}_2\|$. We can solve for the unknown range at either time by using conservation of specific angular momentum and specific orbital energy.

Begin with specific angular momentum,

$$\mathbf{h} = \mathbf{r}_1 \times \mathbf{v}_1 = \mathbf{r}_2 \times \mathbf{v}_2 \tag{2}$$

Rewriting in terms of $\mathbf{u}_1$ and $\mathbf{u}_2$,

$$\mathbf{h} = \rho_1 \left(\mathbf{v}_1 \times \mathbf{u}_1\right) = \rho_2 \left(\mathbf{v}_2 \times \mathbf{u}_2\right) \tag{3}$$

Now, find the magnitude of the specific angular momentum,

$$h = \|\mathbf{h}\| = \rho_1 \|\mathbf{v}_1 \times \mathbf{u}_1\| = \rho_2 \|\mathbf{v}_2 \times \mathbf{u}_2\| \tag{4}$$

to arrive at the following relation between ρ_1 and ρ_2

$$\rho_2 = \rho_1 \frac{\|\mathbf{v}_1 \times \mathbf{u}_1\|}{\|\mathbf{v}_2 \times \mathbf{u}_2\|} \tag{5}$$

Likewise, we have conservation of specific orbital energy,

$$\mathcal{E} = \frac{\mathbf{v}_1^\mathsf{T} \mathbf{v}_1}{2} - \frac{\mu}{\rho_1} = \frac{\mathbf{v}_2^\mathsf{T} \mathbf{v}_2}{2} - \frac{\mu}{\rho_2} \tag{6}$$

where μ is the standard gravitational parameter.

We now have two equations (Eq. 5 and Eq. 6) in two unknowns (ρ_1 and ρ_2). Therefore, substitute Eq. 5 into Eq. 6 to solve for ρ_1 and multiply by $-\mathbf{u}_1$ to get $\mathbf{r}_1$:

$$\mathbf{r}_1 = -\rho_1 \mathbf{u}_1 = -2\mu \frac{\|\mathbf{v}_1 \times \mathbf{u}_1\| - \|\mathbf{v}_2 \times \mathbf{u}_2\|}{\left(\mathbf{v}_1^\mathsf{T} \mathbf{v}_1 - \mathbf{v}_2^\mathsf{T} \mathbf{v}_2\right) \|\mathbf{v}_1 \times \mathbf{u}_1\|} \mathbf{u}_1 \tag{7}$$

Equal Velocity Magnitude Case

Note that the result in Eq. 7 approaches a singularity in cases where the magnitudes of $\mathbf{v}_1$ and $\mathbf{v}_2$ are sufficiently close. This occurs because the equation for specific orbital energy becomes redundant, and so an alternative method is needed.

There are two possible scenarios that would allow $\|\mathbf{v}_1\| = \|\mathbf{v}_2\|$ and $\mathbf{v}_1 \neq \mathbf{v}_2$. The first scenario is a circular orbit. If this were the case, then the velocity vector would be perpendicular to the line of sight such that $\mathbf{v}_i^\mathsf{T} \mathbf{u}_i = 0$. In a circular orbit, the value of $\mathbf{r}$ is simply given by

$$\mathbf{r}_i = -\frac{\mu}{\|\mathbf{v}_i\|^2} \mathbf{u}_i \tag{8}$$

If $\|\mathbf{v}_1\| = \|\mathbf{v}_2\|$, $\mathbf{v}_1 \neq \mathbf{v}_2$, and $\mathbf{v}_i^\mathsf{T} \mathbf{u}_i \neq 0$, then the position vectors $\mathbf{r}_1$ and $\mathbf{r}_2$ must be equal in magnitude and reflected across the line of apsides as shown in Fig. 3.

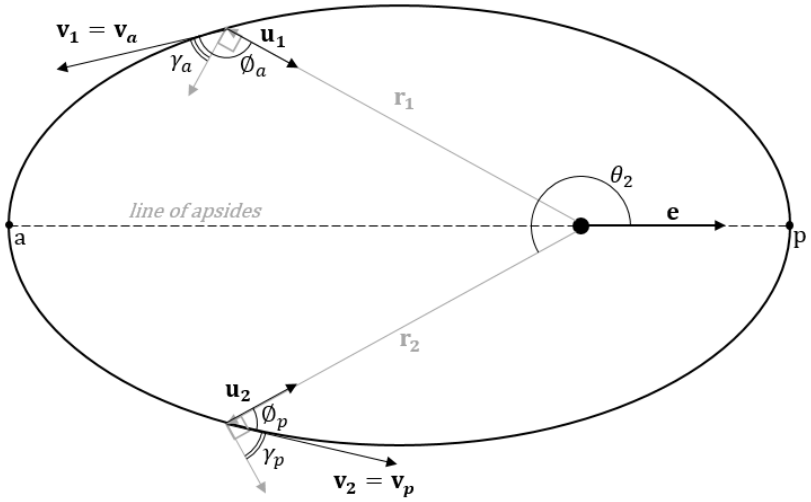

Figure 3. Example orbit geometry when $\|\mathbf{v}_1\| = \|\mathbf{v}_2\|$ and $\mathbf{v}_1 \neq \mathbf{v}_2$. Observe the reflected geometry about the line of apsides.

This geometry can be utilized to fully define the orbit by solving for the eccentricity vector, **e**, whose direction bisects the line-of-sight vectors,

$$\hat{\mathbf{e}} = \frac{\mathbf{e}}{e} = \pm \frac{\mathbf{u}_1 + \mathbf{u}_2}{\|\mathbf{u}_1 + \mathbf{u}_2\|} \tag{9}$$

where the scalar $e = \|\mathbf{e}\|$ is the orbit eccentricity.

The sign of $\hat{\mathbf{e}}$ is such that

$$\hat{\mathbf{e}}^\intercal \mathbf{v}_p > 0 \tag{10}$$

where $\mathbf{v}_p$ is whichever of the two velocity vectors, $\mathbf{v}_1$ or $\mathbf{v}_2$, points towards periapsis. This is the case if the angle ϕ between the velocity vector and the line of sight is less than $\frac{\pi}{2}$. The other will point towards apoapsis (or simply away from periapsis if the orbit is open) and have angle ϕ greater than $\frac{\pi}{2}$, as shown in Fig. 3.

$$\phi_p = \cos^{-1}\left(\frac{\mathbf{v}_p^\intercal \mathbf{u}_p}{\|\mathbf{v}_p\|}\right) < \frac{\pi}{2} \tag{11}$$

$$\phi_a = \cos^{-1}\left(\frac{\mathbf{v}_a^\intercal \mathbf{u}_a}{\|\mathbf{v}_a\|}\right) > \frac{\pi}{2} \tag{12}$$

The flight path angle γ is then given by

$$\gamma_p = \frac{\pi}{2} - \phi_p \tag{13}$$

$$\gamma_a = \phi_a - \frac{\pi}{2} \tag{14}$$

With the direction of the eccentricity vector known, we can determine the true anomaly θ,

$$\theta_p = 2\pi - \cos^{-1}\left(-\mathbf{u}_p^\intercal \hat{\mathbf{e}}\right) \tag{15}$$

$$\theta_a = \cos^{-1}\left(-\mathbf{u}_a^\intercal \hat{\mathbf{e}}\right) \tag{16}$$

The magnitude of the eccentricity vector is a function of the flight path angle and the true anomaly,

$$\|\mathbf{e}\| = e = \frac{\tan\gamma_i}{\sin\theta_i - \tan\gamma_i \cos\theta_i} \tag{17}$$

The full eccentricity vector is then simply

$$\mathbf{e} = e\hat{\mathbf{e}} \tag{18}$$

Finally, the position vector can be found by combining the *vis-viva* equation

$$\|\mathbf{v}_i\|^2 = \mu\left(\frac{2}{\rho_i} - \frac{1}{a}\right) \tag{19}$$

with the orbit equation

$$\rho_i = \frac{a\left(1-e^2\right)}{1+e\cos\theta_i} \tag{20}$$

resulting in

$$\rho_i = \frac{\mu\left(e^2 + 2e\cos\theta_i + 1\right)}{\|\mathbf{v}_i\|\left(1+e\cos\theta_i\right)} \tag{21}$$

so that

$$\mathbf{r}_i = -\frac{\mu\left(e^2 + 2e\cos\theta_i + 1\right)}{\|\mathbf{v}_i\|\left(1+e\cos\theta_i\right)}\mathbf{u}_i \tag{22}$$

PERFORMANCE AND DISCUSSION

The method for IOD from two velocity vectors and their respective lines-of-sight presented in the previous section was validated and assessed through a number of analytic and numerical studies.

Analytic Covariance

It is important to understand how the solution method degrades in the presence of measurement noise. An analytic expression for the covariance of $\mathbf{r}_1$ can be compactly derived from Eq. 7. Taking the Taylor Series to first order,

$$\delta\mathbf{r}_1 = \frac{\partial\mathbf{r}_1}{\partial\mathbf{u}_1}\delta\mathbf{u}_1 + \frac{\partial\mathbf{r}_1}{\partial\mathbf{u}_2}\delta\mathbf{u}_2 + \frac{\partial\mathbf{r}_1}{\partial\mathbf{v}_1}\delta\mathbf{v}_1 + \frac{\partial\mathbf{r}_1}{\partial\mathbf{v}_2}\delta\mathbf{v}_2 \tag{23}$$

Recognizing that $\mathbf{r}_1 = \rho_1\mathbf{u}_1$ and letting $\mathbf{H}_{\mathbf{x}i} = \frac{\partial\rho_1}{\partial\mathbf{x}_i}$, where $\mathbf{x}$ is either $\mathbf{v}$ or $\mathbf{u}$ and i is either 1 or 2, Eq. 23 can be rewritten as

$$\delta\mathbf{r}_1 = \rho_1\delta\mathbf{u}_1 + \left(\mathbf{H}_{\mathbf{u}1}\delta\mathbf{u}_1 + \mathbf{H}_{\mathbf{u}2}\delta\mathbf{u}_2 + \mathbf{H}_{\mathbf{v}1}\delta\mathbf{v}_1 + \mathbf{H}_{\mathbf{v}2}\delta\mathbf{v}_2\right)\mathbf{u}_1 \tag{24}$$

The partial derivatives are as follows:

$$\mathbf{H}_{\mathbf{u}1} = -2\mu\frac{\|\mathbf{v}_2\times\mathbf{u}_2\|}{\left(\mathbf{v}_1^\intercal\mathbf{v}_1 - \mathbf{v}_2^\intercal\mathbf{v}_2\right)\|\mathbf{v}_1\times\mathbf{u}_1\|^3}\mathbf{u}_1^\intercal\left[\mathbf{v}_1\times\right]^2$$

$$\mathbf{H}_{\mathbf{u}2} = 2\mu \frac{1}{\left(\mathbf{v}_1^\intercal \mathbf{v}_1 - \mathbf{v}_2^\intercal \mathbf{v}_2\right) \|\mathbf{v}_1 \times \mathbf{u}_1\| \|\mathbf{v}_2 \times \mathbf{u}_2\|} \mathbf{u}_2^\intercal \left[\mathbf{v}_2 \times\right]^2$$

$$\mathbf{H}_{\mathbf{v}1} = 4\mu \frac{\|\mathbf{v}_2 \times \mathbf{u}_2\| - \|\mathbf{v}_1 \times \mathbf{u}_1\|}{\left(\mathbf{v}_1^\intercal \mathbf{v}_1 - \mathbf{v}_2^\intercal \mathbf{v}_2\right)^2 \|\mathbf{v}_1 \times \mathbf{u}_1\|} \mathbf{v}_1^\intercal - 2\mu \frac{\|\mathbf{v}_2 \times \mathbf{u}_2\|}{\left(\mathbf{v}_1^\intercal \mathbf{v}_1 - \mathbf{v}_2^\intercal \mathbf{v}_2\right) \|\mathbf{v}_1 \times \mathbf{u}_1\|^3} \mathbf{v}_1^\intercal \left[\mathbf{u}_1 \times\right]^2$$

$$\mathbf{H}_{\mathbf{v}2} = 4\mu \frac{\|\mathbf{v}_1 \times \mathbf{u}_1\| - \|\mathbf{v}_2 \times \mathbf{u}_2\|}{\left(\mathbf{v}_1^\intercal \mathbf{v}_1 - \mathbf{v}_2^\intercal \mathbf{v}_2\right)^2 \|\mathbf{v}_1 \times \mathbf{u}_1\|} \mathbf{v}_2^\intercal + 2\mu \frac{1}{\left(\mathbf{v}_1^\intercal \mathbf{v}_1 - \mathbf{v}_2^\intercal \mathbf{v}_2\right) \|\mathbf{v}_1 \times \mathbf{u}_1\| \|\mathbf{v}_2 \times \mathbf{u}_2\|} \mathbf{v}_2^\intercal \left[\mathbf{u}_2 \times\right]^2 \quad (25)$$

The covariance of $\mathbf{r}_1$ is given by

$$\mathbf{P}_{\mathbf{r}1} = \mathbb{E}\left[\delta \mathbf{r}_1 \delta \mathbf{r}_1^\intercal\right] \quad (26)$$

where $\mathbb{E}\left[\cdot\right]$ is the expected value operator.

Let the uncertainty of the line-of-sight measurements be given by the standard unit vector covariance[6]

$$\mathbf{R}_{\mathbf{u}i} = \mathbb{E}\left[\delta \mathbf{u}_i \delta \mathbf{u}_i^\intercal\right] = \sigma_u^2 \left(\mathbf{I}_{3\times 3} - \mathbf{u}_i \mathbf{u}_i^\intercal\right) \quad (27)$$

and of the velocity measurements simply by

$$\mathbf{R}_{\mathbf{v}i} = \mathbb{E}\left[\delta \mathbf{v}_i \delta \mathbf{v}_i^\intercal\right] = \sigma_v^2 \mathbf{I}_{3\times 3} \quad (28)$$

Combining Eqs. 24-28 results in the following analytic expression for the covariance of $\mathbf{r}_1$:

$$\begin{aligned}\mathbf{P}_{\mathbf{r}1} = {} & \rho_1^2 \sigma_u^2 \left(\mathbf{I}_{3\times 3} - \mathbf{u}_1 \mathbf{u}_1^\intercal\right) + \rho_1 \sigma_u^2 \left[\mathbf{u}_1 \mathbf{H}_{\mathbf{u}1} \left(\mathbf{I}_{3\times 3} - \mathbf{u}_1 \mathbf{u}_1^\intercal\right) + \left(\mathbf{I}_{3\times 3} - \mathbf{u}_1 \mathbf{u}_1^\intercal\right) \mathbf{H}_{\mathbf{u}1}^\intercal \mathbf{u}_1^\intercal\right] + \\ & \left\{\sigma_u^2 \left[\mathbf{H}_{\mathbf{u}1} \left(\mathbf{I}_{3\times 3} - \mathbf{u}_1 \mathbf{u}_1^\intercal\right) \mathbf{H}_{\mathbf{u}1}^\intercal + \mathbf{H}_{\mathbf{u}2} \left(\mathbf{I}_{3\times 3} - \mathbf{u}_2 \mathbf{u}_2^\intercal\right) \mathbf{H}_{\mathbf{u}2}^\intercal\right] + \sigma_v^2 \left[\mathbf{H}_{\mathbf{v}1} \mathbf{H}_{\mathbf{v}1}^\intercal + \mathbf{H}_{\mathbf{v}2} \mathbf{H}_{\mathbf{v}2}^\intercal\right]\right\} \mathbf{u}_1 \mathbf{u}_1^\intercal \end{aligned} \quad (29)$$

Numerical Results

Consider an example spacecraft in a heliocentric orbit undergoing perfect two-body motion. The spacecraft is assumed to be in a prograde orbit with periapsis radius of 1 Astronomical Unit (AU), inclination of 30 degrees, argument of periapsis of 70 degrees, and right ascenscion of the ascending node (RAAN) of 40 degrees. Positions for both elliptical and hyperbolic orbits were recovered to within machine precision for both the standard IOD method as well as the special reflected case IOD method. The results from this analysis are shown in Table 1.

A 1,000-run Monte Carlo simulation was done for the same example spacecraft as above for an orbit with eccentricity of 0.4. The standard deviation of the line-of-sight measurements, σ_u, and of the velocity measurements, σ_v, were assumed to be 0.03 degrees and 1 m/s, respectively. The resulting position errors and 3σ error ellipses are plotted in cartesian coordinates in Fig. 4. The analytic and numerical covariance ellipses show clear agreement. Additionally, the semi-major axis and flight path angle errors are plotted in Fig. 5.

The same scenario was used to generate inputs to the covariance expression given in Eq. 29 for a sweep of measurement errors. A contour of the expected error in position in kilometers as a function of measurement uncertainty (where σ_u varies from 0 to 0.05 degrees and σ_v varies from 0 to 10 m/s) can be seen in Fig. 6. It is evident from Fig. 6 that limitations in our ability to accurately centroid the Sun is a major limiting factor in IOD performance. This has led to parallel work by the authors in velocity-only IOD, which doesn't suffer from this problem.

Table 1. IOD-produced positions are correct to within machine precision when all measurements are perfect.

	Orbit Type	Time	True Anomaly	Error, km		
				δr_x	δr_y	δr_z
$\|\mathbf{v}_1\| \neq \|\mathbf{v}_2\|$	Elliptical (e=0.4)	t_1	75 deg	0.2980×10^{-7}	0.0745×10^{-7}	0.0000×10^{-7}
		t_2	128 deg	-0.2980×10^{-7}	-0.2980×10^{-7}	-0.0745×10^{-7}
	Hyperbolic (e=1.2)	t_1	121 deg	0.3576×10^{-6}	0.3576×10^{-6}	0.0447×10^{-6}
		t_2	133 deg	0.1073×10^{-5}	0.1907×10^{-5}	0.0477×10^{-5}
$\|\mathbf{v}_1\| = \|\mathbf{v}_2\|$	Elliptical (e=0.4)	t_1	-75 deg	0.0000×10^{-7}	-0.1490×10^{-7}	0.0186×10^{-7}
		t_2	75 deg	0.5960×10^{-7}	0.1118×10^{-7}	-0.1490×10^{-7}
	Hyperbolic (e=1.2)	t_1	-121 deg	-0.1311×10^{-5}	0.0179×10^{-5}	0.0596×10^{-5}
		t_2	121 deg	0.1073×10^{-5}	0.1311×10^{-5}	0.0164×10^{-5}

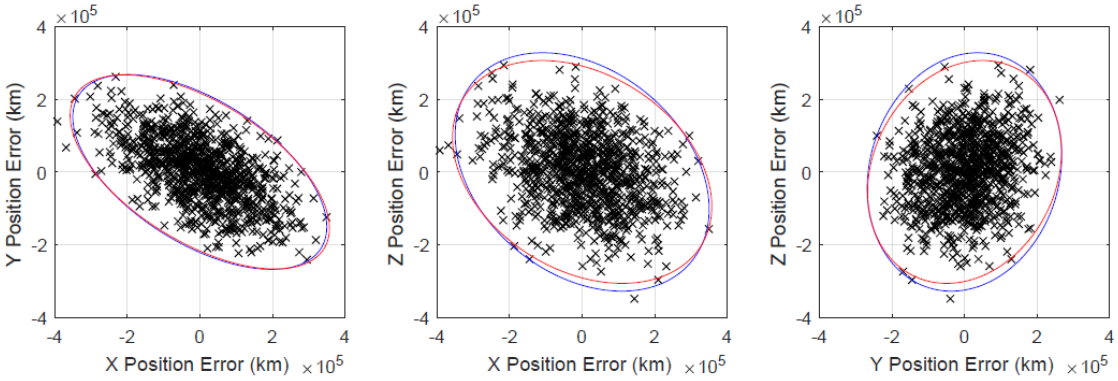

Figure 4. Postion errors and 3σ error ellipses (blue=analytic, red=numeric) corresponding to measurement at t_1 for two velocity and LOS IOD.

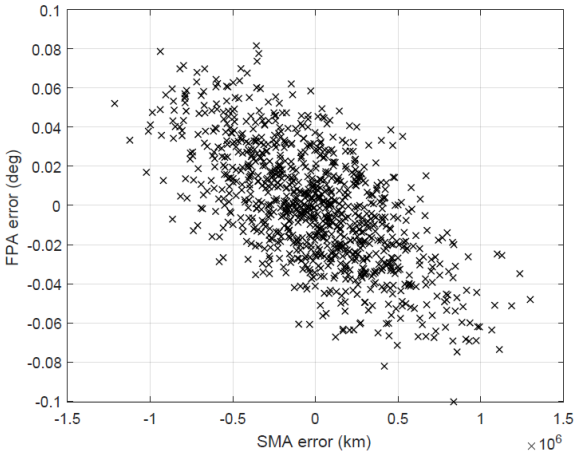

Figure 5. Scatter plot of semi-major axis residuals and flight path angle residuals corresponding to first measurement (at t_1).

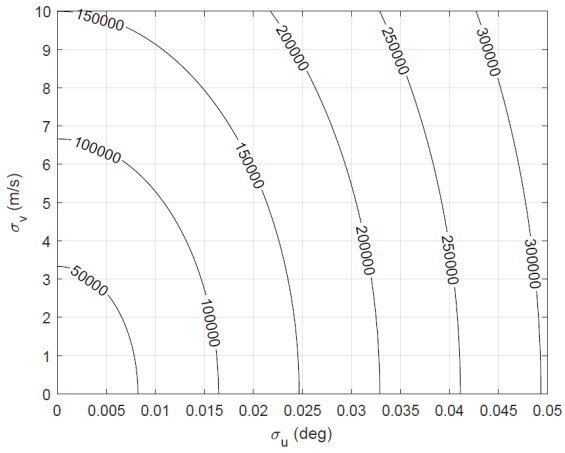

Figure 6. Postion errors in km at measurement time t_1 as a function of varying measurement errors.

CONCLUSIONS

This work considers the problem of initial orbit determination (IOD) given two velocity vectors and lines-of-sight to the central body. This problem is part of a greater set of velocity-based IOD problems that the authors are exploring in parallel lines of work. Although the present work was motivated by velocity measurements from x-ray navigation (XNAV), the IOD approach developed here is valid for any future system capable of obtaining inertial velocity measurements. An analytic solution to the problem of IOD from two velocity vectors and lines-of-sight is derived, along with simple special case checks and methods. The analytic IOD solution works for both closed and open orbits. Numerical studies demonstrate that a computer implementation of this algorithm produces the correct solution to within machine precision for objects undergoing two-body motion and with perfect (noise-free) measurements. The same algorithm is capable of processing noisy measurements, with navigation performance that is dependant on sensor accuracy.

ACKNOWLEDGEMENTS

The authors thank Zach Putnam and Kevin Lohan from the University of Illinois at Urbana-Champaign for insightful discussions on x-ray navigation.

REFERENCES

[1] R. H. Batton, *An Introduction to the Mathematics and Methods of Astrodynamics, Revised Edition*. Reston, Virginia: American Institute of Aeronautics and Astronautics, Inc., 1999.

[2] D. A. Vallado, *Fundamentals of Astrodynamics and Applications*. Hawthorne, CA: Microcosm Press, 3rd ed., 2007.

[3] P. R. Escobal, *Methods of Orbit Determination*. Malabar, FL: Robert E. Krieger Publishing Company, 2nd ed., 1976.

[4] R. Gooding, "A New Procedure for the Solution of the Classical Problem of Minimal Orbit Determination from Three Lines of Sight," *Celestial Mechanics & Dynamical Astronomy*, Vol. 66, 1997, pp. 387–423.

[5] S. I. Sheikh, D. J. Pines, P. S. Ray, K. S. Wood, M. N. Lovellette, and M. T. Wolff, "Spacecraft Navigation Using X-Ray Pulsars," *Journal of Guidance, Control, and Dynamics*, Vol. 29, No. 1, 2006, pp. 49–63.

[6] M. D. Shuster, "Maximum Likelihood Estimation of Spacecraft Attitude," *The Journal of the Astronautical Sciences*, Vol. 37, No. 1, 1989, pp. 79–88.